Arch Appl Mech (2018) 88:175–192
https://doi.org/10.1007/s00419-017-1301-6

SPECIAL

Andrzej Chudzikiewicz · Jaroslaw Korzeb

Simulation study of wheels wear in low-floor tram with independently rotating wheels

Received: 8 January 2017 / Accepted: 5 September 2017 / Published online: 6 February 2018

Abstract This paper presents an example of low-floor trams simulation tests. The tram under study was unique because of using the system of independently rotating wheels in the bogie IRW ("Chudzikiewicz et al., in: The structural design of a modern, completely low-floor tram with independently rotating wheels (Report in Polish) NCBiR—DEMONSTRATOR+, Warsaw University of Technology Faculty of Transport—PESA Bydgoszcz, 2014"). In this paper, the dynamic behavior of the vehicle was examined, and the phenomenon of wheels and rails wear, during the rolling contact, was subjected to the identification. For this purpose, a dedicated computational model was built in MATLAB environment, taking into account the phenomenon of kinematic pair wear using Archard's model.

Keywords Transport · Exploitation · Friction · Contact forces · Wheels wear · IRW

1 Introduction

The migration of society and the development of cities require the modification of existing transportation networks in urban areas. The introduction of new communication pathways and more effective means of transportation is essential. The development of rail transportation, which moves atop dedicated tracks, constitutes an important element of effective passenger transport [2,3]. The classical approach to the construction of tram wagons results in varied floor levels among their different types. Effects of this include unused space and limited access to specific sections of the tram for disabled people; hence, the construction of entirely low-floor trams seems to be a good solution. Such a construction fulfills the expectations of elderly people with limited mobility, does not require an overhaul to city infrastructure or only requires lesser modifications to it, and facilitates the movement of passengers within the vehicle [1].

Trams equipped with independently rotating wheels are appropriate solution of railway vehicles allowing the construction of low-floor vehicles, having more free space above bogies driving gear (Fig. 1).

In this work, studies were conducted upon a tram made up of five segments, equipped with three wagons, the outer two of which were used as driving gear. All bogies were equipped with independently rotating wheels. The completely low-floor tram was designed as a key element in the practice implementation of the project [1].

Suitable model of the wheelset and degrees of freedom is shown in Fig. 2.

A. Chudzikiewicz · J. Korzeb (✉)
Faculty of Transport, Warsaw University of Technology, 75 Koszykowa Street, 00-662 Warsaw, Poland
E-mail: korzeb@wt.pw.edu.pl

A. Chudzikiewicz
E-mail: ach@wt.pw.edu.pl

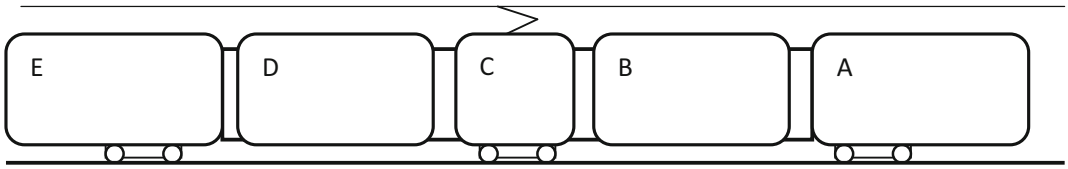

Fig. 1 A model of the low-floor tram, based on [1]

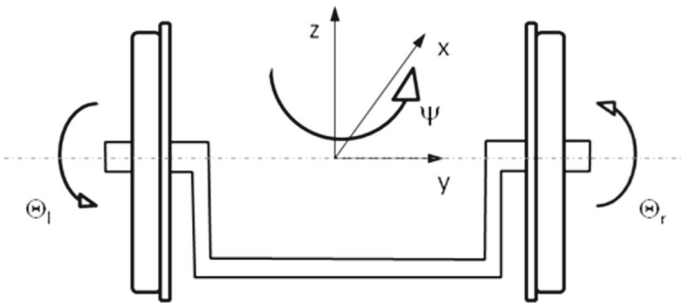

Fig. 2 A model of the wheelset and degrees of freedom [1]

To increase the driving speed and the passenger capacity of the trams, the appropriate levels of safety and comfort must be maintained. The driving safety is determined by the wheels of the running gear, or more specifically, the phenomena taking place between the wheels and the railway track [4–6]. The state of the profiles of the wheels and rails plays principle roles in determining the safety and comfort of travel. It also influences the speed limit of the vehicle in regular operating conditions. The phenomenon of the wearing down of the wheel and rail profiles during the usage of rail vehicles has been studied for years, and the studies concentrate on the precise recognition of the phenomena taking place in the contact zone between the wheel and rail.

Many theoretical and experimental studies (Kalker, Chudzikiewicz, Zobory, Piotrowski, Knothe, Bohn, Nilsson, Nowakowski and others) adopted the Archard model as a basis for the wear of the profiles of wheels and rail [6–12]. This model assumes a proportional relation between the work of friction and the total wear in the contact zone and uses Coulomb's model of friction [13]. Moreover, this model does not include heat or dynamic phenomena in the contact zone.

2 The phenomena in the contact zone

In case of two solid bodies contact, literature considers many theories taking into account phenomena in the contact area on a surface. Restraining force (frictional force) is directly proportional to the pressure force and depends on the parameters of the rubbing surfaces: material type, surface roughness, the temperature of the surroundings, environment properties (occurrence of external factors that reduce or increase the friction), and the state of movement (sliding or rolling friction) [7,14,15].

In the case of metals and their technical alloys, the forces associated with the contact area generate stresses, giving in consequence the elastic deformation of surface. After crossing the plasticity limit, the strengthening of material can occur by distortion of crystal structure, which translates into an increasing of hardness and strength and reducing the plastic properties. As a result of internal friction and internal energy dissipation due to the tension and compression, the relation describing the deformation as a stress function is nonlinear and takes the form of hysteresis, called elastic hysteresis. The ratio of the latter quantity over the elastic deformation energy represents the vibration reduction capability. The tribological material wear due to the friction is caused by abrasion, cracking, material defects, adhesion of the contact surfaces, and tribochemical reactions [7,14,16–18].

Regarding the contact between two solids, the literature considers friction phenomena in a contact zone on a surface, called that the formation of a force counteracting the movement, directed in the opposite direction of body's movement. In the case of a railway wheel and rail, a pure roll practically never occurs, that's why the occurrence of micro-slips leads to the creation of forces of friction (tangential contact forces) and their moments in the contact zone [19–21]. It should be noted that complex type of slippage has been included in

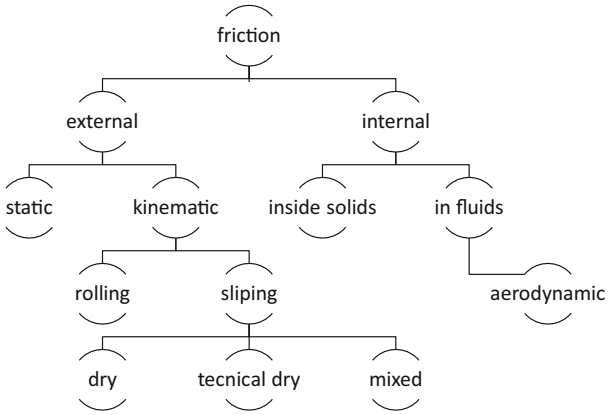

Fig. 3 A classification of frictions [1,20]

procedures for tangential forces calculation in contact area of wheel–rail kinematic pair. In the first phase, the contact areas were determined, later the slip, and tangential forces. Moreover in the contact area occur the longitudinal creepage, lateral creepage, and the spin creepage, and they were calculated in every iteration. The contact forces are one of the most essential elements determining the intensity of the surfaces' wear. Their value is a nonlinear function of the micro-slip and also depends on other variables such as material properties, the value of the coefficient of friction, the value of normal forces, and the geometry of the contact, and this is the concept of wear caused by the processes of friction. Within this conception occurs decreases the mass, and change physical surface properties of the contact zone.

Wear processes that are not caused by friction can be named corrosion, erosion, cavitation, thermal fatigue, and others. An analysis of the occurring phenomena is presented in the following subchapters.

2.1 The phenomenon of friction

The braking force (friction) is directly proportional to the force of pressure and depends on the parameters of the rubbing surfaces: the material, the surface roughness, the ambient temperature, the environment (occurrence of factors increasing or decreasing friction), and the state of movement (sliding friction, rolling friction) [20,22]. They are classified in the diagram below. Emphasized are constructional, lubricated, and mixed friction (Fig. 3). Selected types of friction:

- External friction (during surface contact of the bodies; its value depends on the composition and structure of the materials),
- Kinetic friction (occurs during contact between surfaces in relative movement),
- Sliding friction (occurs when the velocities of the rubbing bodies in the contact zone are different),
- Dry friction (occurs when the rubbing surfaces are not separated by a third body and touch directly),
- Lubricated friction (the surfaces in contact are oxidized, or are covered in a layer of liquid or gas).

It is important to note that the force of sliding friction is proportional to the normal force component keeping the bodies in contact, has no relation with the area of the bodies' contact zone, and is independent from velocity when in motion. The parameters characterizing friction in rolling motion are the strength, moment, coefficient of rolling friction and rolling resistance, which are described in Sect. 2.1.2. In this subchapter, internal friction in solids as well as external, kinetic, sliding, and rolling friction will be further analyzed as causes of tribological wear.

2.1.1 Internal friction

As a result of internal friction and the internal diffusion of energy caused by stretching and squeezing, the relation describing the deformations in the tension function is not linear—it takes the form of a hysteresis, namely an elastic hysteresis, which represents the capacity to dampen vibrations when divided by the energy of the plastic deformation. The main causes for the occurrence of internal friction are defects in crystal structure, the intrusion of alien atoms (i.e., excess atoms), or displacements on crystallites boundaries [9,12,17,23].

Resistances to internal friction depend on, among others:

- The chemical composition,
- The type of heat treating,
- The type of forming processes,
- The magnitude of crushing,
- The temperature,
- The density of existing defects in the crystal structure,
- Existing internal tensions.

Internal friction is influenced by mechanisms related to defects in the crystal structure and their migration, dislocations caused by their vibrations and movements, and thermoelastic relaxation.

2.1.2 External friction

External friction occurs in the case of surface contact between two bodies and can be categorized as static friction or kinetic friction (the bodies remain in relative movement, e.g., sliding friction—at varying body speeds in the contact zone) based on their relative velocities.

The condition of the external surface—the contact of elements characterizes waviness, structural errors, and the direction of the arrangement of irregularities. While examining the rubbing surface with external—kinetic friction, the following must be taken into account:

- The contoured contact surface (the area of the contour of the actual contact zones, a function of roughness, waviness, and load),
- The actual contact surface (the sum of elementary contact surfaces),
- The nominal contact surface (within the boundaries of the contour of the contact zone, a function of nominal geometric dimensions),

The real effect of rubbing surfaces depends on the surface of contact and its condition as well as the physical properties of the rubbing elements' materials. A factor influencing rolling friction is the creation and tearing of bridge (adhesive) connections between the bodies [20].

Bowden and Tabor [24] reported the adhesion theory of friction, which assumes the contact of the bodies on a real plane, resulting from the unevenness of the real contact zone, which leads to the formation of contacts named *short-circuit bridges*. Tomlinson [25] and Deriagin [26] described different approaches, which was named the molecular theory of friction. This theory assumed the effect on the internal force of friction caused by intermolecular forces, between the electron shells of the atoms of the adhering bodies. Kragielski [27] prepared continuation of this theory in the form of an adhesion–deformation approach and paid special attention on necessity of connection the influence of mechanical unevenness of the real surface of contact with molecular attraction [31]. Kostecki [28] described the energy balance of the processes of external friction has strong connection with thermal and acoustic phenomena losses in energy, and corrugation processes. In accordance with this theory, it is possible to calculate the work of friction forces as a sum of energetic components, and in the case of external friction, it is equal to the thermal energy and dissipation. In the case of rolling contact, there exist hypotheses (e.g., [22]), from which it follows that loading a contact surface with a turning moment causes two types of behavior:

- Abrupt tearing of adhesive bridges along with the instantaneous formation of new connections,
- Relaxation of the friction forced caused by creep, just like with viscoelastic connections (probably caused by a accumulation of defects (e.g., vacancies) in the surface layer [22].

By generalizing the above theories, it must be stated that, from an analytical point of view, the effect of friction is the diffusion of energy.

The assumed typical values for the friction coefficient for the wheel–rail pair used for calculation are presented in Fig. 4.

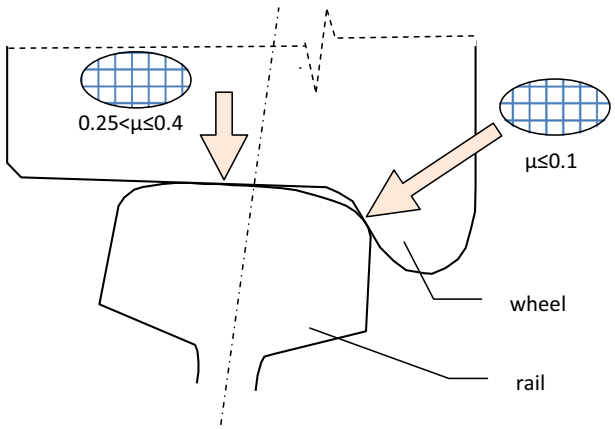

Fig. 4 Coefficient of friction in the wheel–rail contact area

The generalized form of the friction model is in accordance with Coulomb's theory, taking into account viscous friction [20,29]:

$$T\dot{x} = c\dot{x} + N \cdot \mu \cdot \text{sign}(\dot{x}) \tag{1}$$

wherein:

c Coefficient of viscous friction,
$\dot{x}$ The relative velocity of the bodies,
N The normal force,
μ Coefficient of friction.

In the analysis of the theory of friction, it is impossible to omit the effect observed by Stribeck [30], whose research demonstrated the reduction in friction forces along with the growth of relative velocity of the bodies (for low-velocity slips).

2.2 Material analysis

In accordance with the guidelines of Polish Standard "PN-K-92016 *Processed rims (in polish Obręcze obrobione)*", the material used in the production of the rim is hypoeutectoid steel with 0.65–0.75% carbon content. This type of steel belongs to the pearlite–ferritic group with a large prevalence in pearlite, which are characterized by high resistance and hardness, a resistance to abrasion, and a lower ductility thanks to its microstructure composed of plates of cementite in a soft ferritic warp.

The main component influencing the properties of steel is carbon. Increasing its content causes an improvement in resistance properties and increases hardness.

Silicon hardens ferrite, which unfavorably influences ductility. Reducing the thickness of the cementite plates improves susceptibility to elastic deformations and improvements to impact resistance, and the smaller the gaps between the plates, the greater the resistance to abrasive wear.

Manganese influences the hardening of ferrite and causes a decrease in transformation temperature from austenite to pearlite, which in turn causes the excretion of crushed pearlite. The properties of steel are also affected by the distance between the cementite plates in the pearlite (which is a function of carbon content in the austenite grain as well as of the temperature and speed of the eutectoid transformation) and the thickness of these plates, the size of the pearlite colonies, as well as the original dimensions of the austenite grain before cooling. This translates directly into increasing yield strength ($R_{p0,2}$), tensile strength (R_m), and hardness.

In the case of an addition of chrome, it is possible to lower the temperature of the pearlite transformation, which would cause a fragmented pearlite structure that would further improve the resistance properties of steel.

To improve the durability of pearlite structure steels with higher carbon content, pearlite morphology shaping procedures tied to influencing the parameters of heat treatment—isothermal annealing [17]. Tribological experimental studies lead by National Research Centres (PSl. Gliwice, Poland) demonstrate the greatest wear of steel friction pairs after hot rolling (inter-plate distance around 0.28μm) as well as a greater resistance to abrasive wear after isothermal annealing (inter-plate distance of approximately 0.12–0.17 μm) [16,17].

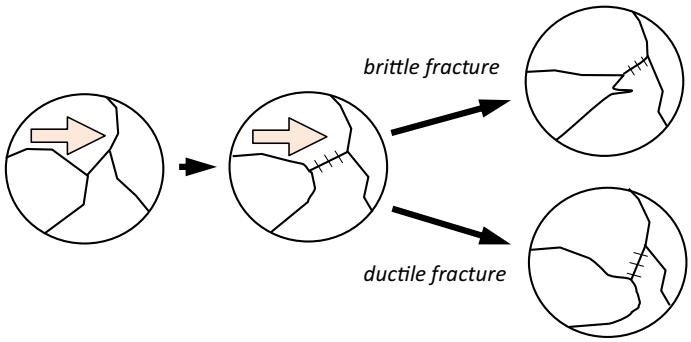

Fig. 5 Mechanism of damage formation as a result of adhesion, based on [15]

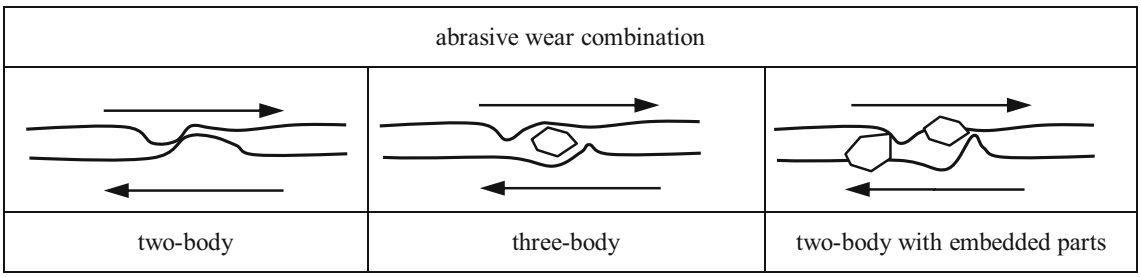

Fig. 6 Mechanism of damage formation as a result of abrasion, based on [15]

2.3 The wear mechanism

The wear of a material as a result of a friction process (tribological) is caused by abrasion, cracking, loss of material, the adhesion of contact surfaces, and tribochemical reactions. Tribological wear and its mechanisms can be classified as [1]:

- Abrasive wear, tied to surface roughness, results in the occurrence of loss of material through cutting,
- Adhesive wear; the adhesion of the surface generates coupling areas, and the effects of motion are fractures,
- Chemical wear, as a result of chemical reactions, e.g., the oxidation of a surface,
- Erosive wear, resulting from other particles hitting the surface of the material,
- Fatigue wear, caused by cyclical deformations of the outer layer, which results in the formation of micro-fissures and fragmentation,
- Heat wear, resulting from energy dissipation in the form of heat having an influence on the properties of the outer layer.

During the friction process in real conditions, apart from coupling with the unevenness of the surface, a change in properties of the outer layer occurs. The notion of the outer layer encompasses the layer of material bounded by the real surface of the object as well as the deeper layer of material, for which a change in physical and chemical characteristics caused by usage can be noted, relative to their equivalents of the undeformed material [22]. Figure 5 depicts the damage formation mechanism caused by adhesion at the crystallites boundaries of the metal.

The motion of rail vehicles in regular usage can be examined as sources of influence of large dynamic loads of a cyclical nature, which translates to destruction in the form of abrasive and fatigue wear and changes in shape and dimensions of the outer layer [15,22,31].

A change in profile of the wheel and rail translates directly to increasing the friction coefficient between the elements of the pair, which leads further to increasing friction forces and shear stress. The mechanism of the formation of damages as a result of abrasive wear is presented in Fig. 6 .

The worn material may have a form of debris that can be moved from one surface to another as a result of adhesion or a local plasticity deformation. Many mechanisms that influence the speed of wear exist. From the speed classification point of view, the literature separates wear into mild (removing small fragments of material, often oxide surfaces), heavy, and catastrophic. This classifying separation is shown in (2) as a standard function of sliding (s_v) and a wear factor (w_f) [15].

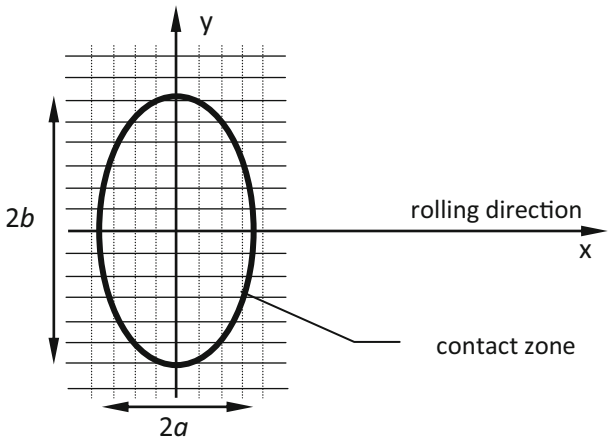

Fig. 7 Discretization of contact area

$$\text{wear} = \begin{cases} s_v \in (0.00 \div 0.03\rangle \,\&\, w_\text{f} \in (0 \div 0.75\rangle \rightarrow \text{mild} \\ s_v, \in (0.03 \div 0.15) \,\&\, w_\text{f} \in (0.75 \div 1.00) \rightarrow \text{heavy} \\ s_v \geq 0.15 \,\&\, w_\text{f} \geq 1.00 \rightarrow \textit{catastrophic} \end{cases} \tag{2}$$

The speed of wear increases as a result of increasing normal load, velocity, and temperature in the contact zone. Description of the process of wear in rolling contact requires assuming the appropriate wear simulation model, taking into account material properties as well as the mechanical influences in the contact zone. The result of the simulation studies is the wear of wheel depth distribution and the speed of wear (quantity of material that is removed per unit of time or per traveled distance). The normal wear process progresses relatively slowly as the oxidation of surfaces, but accelerated wear occurs during the adhesive wear of the border of the rail or wheel caused by friction forces. The type of speed of wear process depends on a combination of contact conditions such as well as the velocity of the vehicle or the contact tension, and climate conditions.

2.4 The adopted model of friction in a contact zone and wear modeling

During the study of the tribological wear phenomena, a lot of computational models were used. The classical approach describes the use of an adhesive model by Archard [18], wherein the volume and weight of material wear (in wear equation) describe the relation:

$$\begin{cases} V_\text{w} = x \cdot k \cdot \frac{N}{H} \\ m_\text{w} = w_\text{r} \cdot \frac{W_\text{f}}{s_\text{c}} \end{cases} \tag{3}$$

wherein:

V_w The volume of the worn material (m^3),
x The distance travelled by the body (m),
k The coefficient describing the probability of a fragment of material tearing off,
N The normal force (N),
H The hardness of the material (MPa),
m_w The mass removed as a result of wear ($\mu\text{g/mm}^2$),
w_r The coefficient of wear (μg/N mm),
W_f The work done by friction forces (N mm),
s_c The area of the surface of contact (mm^2).

In the study of dynamics, modeling of rolling contact with the rail wheels, and the calculation of forces acting at the contact area are crucial. The simplified theory that is applied in the FASTSIM algorithm is based on *band theory* and is limited to a contact zone in the shape of an ellipse, see Fig. 7.

When adhesion area of solids is not large, to make the calculations of contact forces according to the theory for non-conformal contacts, commonly used algorithm for calculating the tangential forces—FASTSIM

developed by Kalker [32] is used. FASTSIM is also successfully used for wear prediction of wheel and rail profiles—Chudzikiewicz [6]. It uses assumptions from Hertzian contact theory [5]:

- A flat contact surface,
- An elliptic distribution of tensions in the contact zone,
- The contact surface is divided into parallel longitudinal bands and a length along the x-axis dependent on the dimensions of the ellipsoid,
- The bands are divided into the same number of elements,
- The calculation of tensions begins from the edge of the ellipsoid for the following elements,
- Slips are calculated relative to the geometric center of the ellipse,
- Constant c_{ij} Kalker [32] coefficients are present over the entire contact surface,
- The c_{ij} values are selected based on the A/B and b/a parameters.

For the purposes of IRW, the FASTSIM procedure (for conventional sets) must be modified to calculate the sliding velocities at the points of contact. This procedure takes into account wear, resulting from contact between two bodies in motion, which is directly proportional to the work done by friction forces in the contact area [29]. The above relation does not take into account friction coefficients, but in the case of tribological wear for rolling contact, they are taken into account in this energetic relation:

$$E_{\mathrm{f}} = \frac{1}{v_{\mathrm{veh}}} \left(F_{\xi} \cdot v_{\xi} + F_{\eta} \cdot v_{\eta} + M_{\varphi} \cdot \omega \right) \tag{4}$$

wherein:

E_{f} The energy of friction forces per unit of travelled distance (J/m),
v_{veh} The velocity of the vehicle (m/s),
F_{ξ} The longitudinal component of the net micro-slip force (N),
F_{η} The lateral component of the net micro-slip force (N),
v_{ξ} The longitudinal micro-slip velocity (m/s),
v_{η} The lateral micro-slip velocity (m/s),
M_{ϕ} The moment in the contact surface (Nm),
ω The angular velocity in the micro-slip area (1/s).

The normalization of the longitudinal, lateral, and angular velocities with the velocity of the vehicle introduces coefficients describing longitudinal, lateral, and spin micro-slips. In the wear process, the following stages can be differentiated: material fatigue, gap initiation, propagation, and removal of metal fragments that lost cohesion.

Wear caused by spalling (or its more advanced version, shelling) is based on the gradual increase in cyclical contact tensions in the outer layer of the rubbing elements for rolling with slipping or without it, during a dry contact within Hertzian tension limits, resulting on the formation of micro-gaps and propagation, which result in the disjointing of material fragments [13]. Wear through pitting is a type of fatigue wear caused by the cyclical occurrence of contact tension, created in the outer layers of rolling elements, for a contact lubricated with a liquid within Hertzian tension limits.
Wear of the wheel or rail can be obtained in two ways:

(a) based on the mass of the worn material (in kg), the wear is proportional to the work done by friction forces in contact point, the unit of work is then: N mm,
(b) based on the depth of the wear's profile (in mm), the wear is proportional to the work done by friction forces on a unitary contact surface, the unit is then N/mm.

It can be written that:

$$m_{\mathrm{w}} = C \cdot W_{\mathrm{r}} \tag{5}$$

m_{w} The mass of worn material in a unitary contact zone (μg/mm^2),
C The wear coefficient (constant) (μg/Nmm),
W_{r} The work done by friction forces in a unitary contact zone (N/mm).

Worn mass [W_{m}, (μg)] and the wear depth [W_{d}, (mm)] can be obtained:

$$W_{\mathrm{m}} = C \times W_{\mathrm{ff}} \tag{6}$$

$$W_{\mathrm{d}} = C_1 \times W_{\mathrm{ff\_ua}} \tag{7}$$

wherein:

C The constant [μg/N mm], $C = \sim 0.00124$ [μg/N mm] (based on Kalker, and Chudzikiewicz simulation calculations [6])
W_{ff} Work done by friction forces [N mm],
C_1 The constant (mm^3/N mm), $C = \sim 1.55 \times 10^{-7}(\mathrm{mm}^2/\mathrm{N})$;
$W_{\mathrm{ff\_ua}}$ Work done by friction forces per unit of area (N/mm).

The relation between constants C and C_1 is the following:

$$C_1 = (1/\rho)\, C \tag{8}$$

wherein ρ is the density of the material (for steel $\rho = 8 \times 10^3$ kg/m^3).
In contact zone, these constants will be the basis of the simulation analysis of the wear model of the wheel and rail profiles, in simulation model. The review of applied models can be found in [5,31].

3 Simulation studies

In real conditions, when the wheel is slipping due to friction, the shape and size of the contact zone as well as the distribution of contact pressures will have influence on contact forces generated between the wheel and rail. After solving the normal contact problem (with delineating the contact zone), the contact problem must be solved using Hertzian theory, with the following assumptions [1,11]:

- The objects' materials are homogeneous, isotropic, and linear elastic,
- Friction does not occur between the surfaces of the objects,
- The objects' surfaces are smooth, and the shape of an undeformed surface can be described with polynomials of the second degree,
- The objects' surfaces' deformations are tied to the surfaces' normal load as described by the Boussinesq function for elastic half-spaces,
- The sizes of the contact zones are small relative to the main radii of the curvatures of the undeformed objects' surfaces.

According to Hertz theory, with above assumptions, the contact zone and the distribution of contact pressure have the shape of an ellipsis with semi-axes a,b dependent on:

- The normal force,
- The objects' material constants,
- Curvatures' their radii.

The Hertzian assumptions are usually not applicable in real conditions, but, despite this, the theory is often used because of the speed of the calculations, as well as the satisfactory precision of the results. Otherwise for the solution of non-Hertzian contact problems, there also exist more complex algorithms [10,11]. Tangential contact problems, of which one of the simplest is Kalker's linear theory, allow for the calculation of tangential forces as linear functions of relative slips. Based on this theory was the FASTSIM algorithm, which is widely used in computer programs that calculate the values of tangential forces in rolling contact zones [1,6,13,29,32].

3.1 The programs used

The next stage of the study regarding the wear on the wheel profile was multivariate simulations conducted with the MATLAB environment package. For simulation studies of motion over straight tracks, the in-house code WearDyn 2014 was used, implemented in the MATLAB environment [1]. The program was built in the MATLAB environment and its work was controlled in more recent environments such as MATLAB 2012. The program is built in a modular fashion, as a main program referring to subprograms saved as m files making calculations or containing functions. The program execution, the control of calculations, the change of parameters, and the launching of simulation calculations are all done through a graphical user interface (GUI) (Fig. 8).
The following information is displayed on the GUI's main dashboard:

- The number of the wheelset's full rotations,
- The longitudinal speed of the set in (m/s) and (km/h),

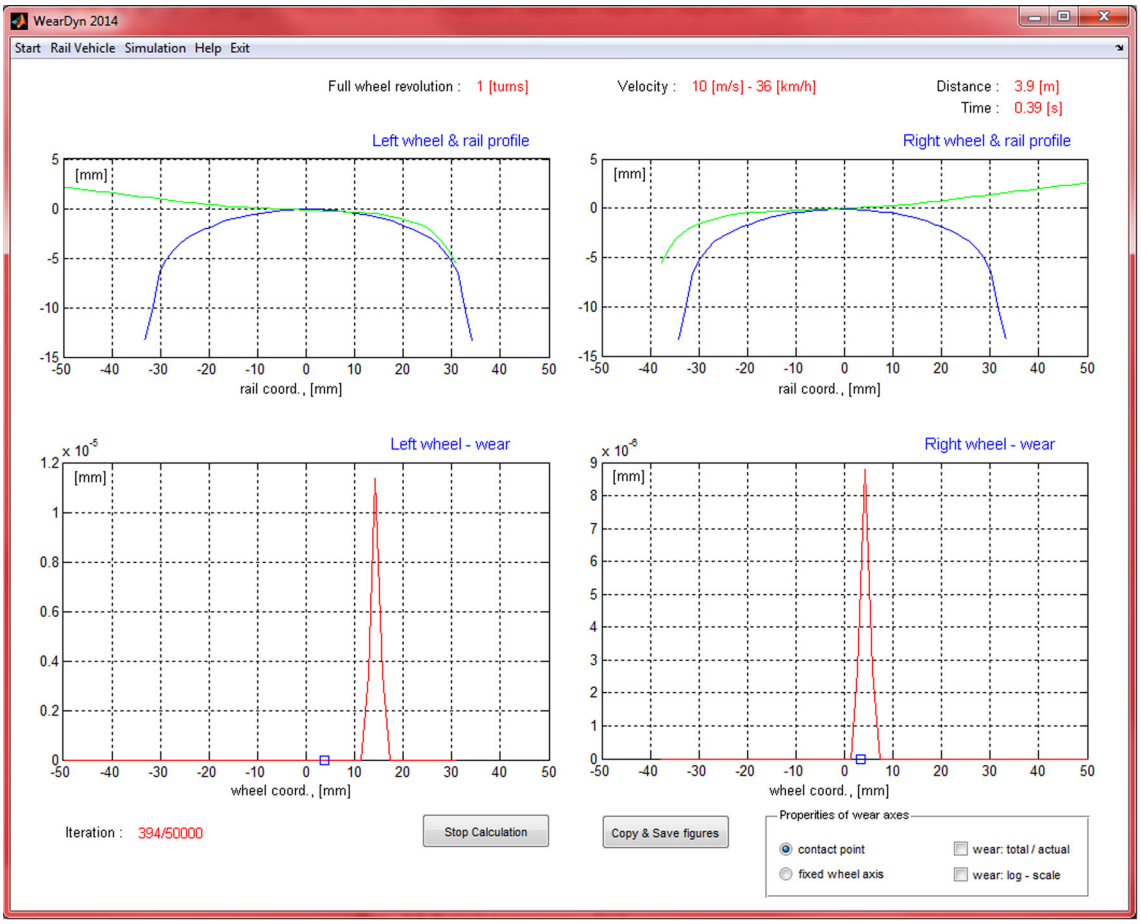

Fig. 8 The GUI dashboard [1]

– The distance travelled based on the number of full wheel rotations,
– The iteration number with respect to the number planned in the series,
– Windows displaying the current profiles and position of the wheels relative to the rails for the left and right sides,
– Windows displaying the current wear of the left and right wheels with the possibility of displaying the total wear (after selecting the "wear: total/actual" option).

The frame of reference of the upper graphs is tied to the PGS (the highest point of the rail head), whereas that of the lower graphs is tied to the set's wheel. When plotting the instantaneous values (wear: actual), the rail head trace is plotted in the form of a blue marker. The wear is plotted in millimeters of loss in the wheel profile, in a linear or logarithmic scale (wear: log-scale). The axis of the cutoff wear charts is tied to the wheel, and the graph can either follow the contact point or be tied to the coordinates of the wheel in a Cartesian system.

Selecting the *Stop Calculation* button causes the interruption of iterative calculations. After that, entry data must be reloaded through the Menu—Start option. Selecting the *Copy & Save figures* button causes all current graphs to be saved as bitmaps in the program's working directory.

Table 1 List of examples of steel used for the production of rails and wheels, with the percentage ranges of the individual components in the alloy ([1], based on PN-EN 13674)

Steel		Rail: RI60N, 180P/S, 49E1 (S49)				Wheel rim: T, PST	
		R260/900A		St80P		P70	
Component	ρ (g/cm^3)	Content (%)		Content (%)		Content (%)	
		From	To	From	To	From	To
Fe	7.87	97.280	98.600	96.960	97.690	97.820	98.530
C	3.51	0.600	0.820	0.530	0.660	0.650	0.750
Mn	7.44	0.650	1.250	0.850	1.150	0.650	0.950
Si	2.33	0.130	0.600	0.850	1.150	0.150	0.400
P	1.82	0.010	0.025	0.040	0.040	0.010	0.040
S	2.06	0.010	0.025	0.040	0.040	0.010	0.040
Density of alloy (g/cm^3)		7.83	7.79	7.79	7.77	7.83	7.81

Table 2 A list of rail steel parameters in accordance with PN-EN 13674-1:2011

Steel	R_m	A	HBW	
	(MPa)	(%)	From	To
R200	680	14	200	240
R220	770	12	220	260
R260	880	10	260	300
R260Mn	880	10	260	300
R320Cr	1080	9	320	360
R350HT	1175	9	350	390
R350LHT	1175	9	350	390
R370CrHT	1280	9	370	410
R400HT	1280	9	400	440

3.1.1 The model parameters

Modeling the usage wear of the wheel–rail system requires the adoption of an additional set of parameters, both material and geometric, characterizing the contact zone and the elements of the analyzed system. To model the wear phenomena of the wheels and the rail surface, sets of material parameters were adopted based on the guidelines of Polish Standard PN-EN 13674-1:2011, which are shown later. Additionally, it is necessary to adopt the formal parameters that control the simulation, as well as to prepare the appropriate entry data packages that characterize:

- The starting profiles of the wheel and rail,
- The maintenance condition of the rail and the lateral unevenness resulting from it,
- The velocity of the vehicle, the static pressures of the wheelsets on the rail, etc.

The parameters characterizing the physical and chemical properties of the material used in the production of the wheels and rail (straight-T, curvilinear-PST profiles) are shown in the table below. In practice, the final content of alloy components, and their proportions depend on the manufacturer of the steel, and the individual order of the railroad owner, depending on the destination of the road (Table 1).
The Rail Vehicles Institute TABOR (Poznan, Poland) has developed a PST tram profile in the mid of 1980s, for the new high-speed tram line. With a wheel width of 90 mm, the thickness of the wheel flange was reduced regard to T-profile, and the combined radius of curvature of the rolling surface was introduced. The circular shape of the working part (rolling surface) of the PST profile results in centering force derived from gravitational forces, and therefore, this profile is also beneficial for vehicles with independently rotating wheels.
The parameters characterizing tensile strength (R_m), relative elongation after fracturing (A), and HBW in the Brinell scale for pearlitic rail steels are listed in Table 2.
In order to prepare the wear model, the following set of parameters had been adopted (Table 3).

Rigidity modulus was used to the numerical calculation, as representation of the wheel and rail properties, together with Poisson's ratios for mentioned elements of kinematic pair, as a description of the elasticity of the contact phenomena according to the FASTSIM structure (the contact problem elasticity description in the

Table 3 The adopted (selected) set of material and geometric parameters [1]

No.	Parameter		Description
	Value	Unit	
1	0.28	–	Poisson ratio of the wheel and rail material (usually for steels 0.27–0.3)
2	7.82×10^3	kg/m^3	Density of the material of wheel rims (usually for wheel steel 7.81–7.83 g/cm^3) according to PN-K-92016
3	82.00	GPa	Modulus of rigidity for the wheel and rail material
4	7.80×10^3	kg/m^3	Density of the rail material (depending on type 7.77–7.83 kg/m^3)
5	0.28	–	Coefficient of friction between the metal surfaces
6	0.66	m	The nominal diameter of the rolling wheels
7	70.79	kN	Static force interactions of a single wheelset on the track in the bogie in segment A
8	61.59	kN	Static force interactions of a single wheelset on the track in the bogie in segment C
9	72.90	kN	Static force interactions of a single wheelset on the track in the bogie in segment E

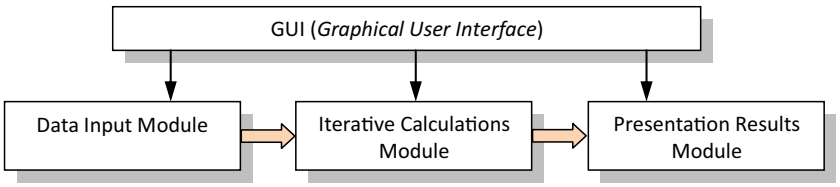

Fig. 9 Simulation model of the wear process—functional structure

framework of the Hertz theory). Young's modulus and the yield point of the material were not directly involved in this procedure.

Determination of stresses in the contact area was only an intermediate step, at each step of computational iteration, since the dimensions of the elemental surfaces in the contact area are known, as well as the distribution of tangential and normal forces for each surface. Calculations for each surface are implicitly present in the program code, but inside interim results, stress distribution was not presented explicitly formally.

3.1.2 The program's algorithm

The structure of the functional simulation model of the wear process is composed of the following elements:

- The control layer
- The data preparation module
- the simulation calculations module
- The results presentation module

Figure 9 shows a flowchart representing the model structure, taking dataflow into account and marking control signals.
The data preparation module is represented in the next figure. This model comprises of (Fig. 10):

- A geometric parameter loading block for the rail and wheel,
- A material parameter loading block,
- An input wear parameter preparation stage,
- A stage for loading characterizing parameters for the wheelset and its motion,
- A simulation parameters loading block.

The next figure shows the simulation calculation module's algorithm, which comprises of (Fig. 11):

- Contact ellipse geometry calculation blocks,
- Force and movement determination blocks,
- Blocks calculating the deformed area, penetration, and friction forces and their work,
- Blocks updating the wheel rim profile with the calculated tribological wear.

The elements connected by the dotted lines represent output data of the algorithm blocks, which are used as input data of the current calculations or other procedures.
The wear calculation program contains a module presenting results. Because of the nature of the received results, they can be presented in the form of:

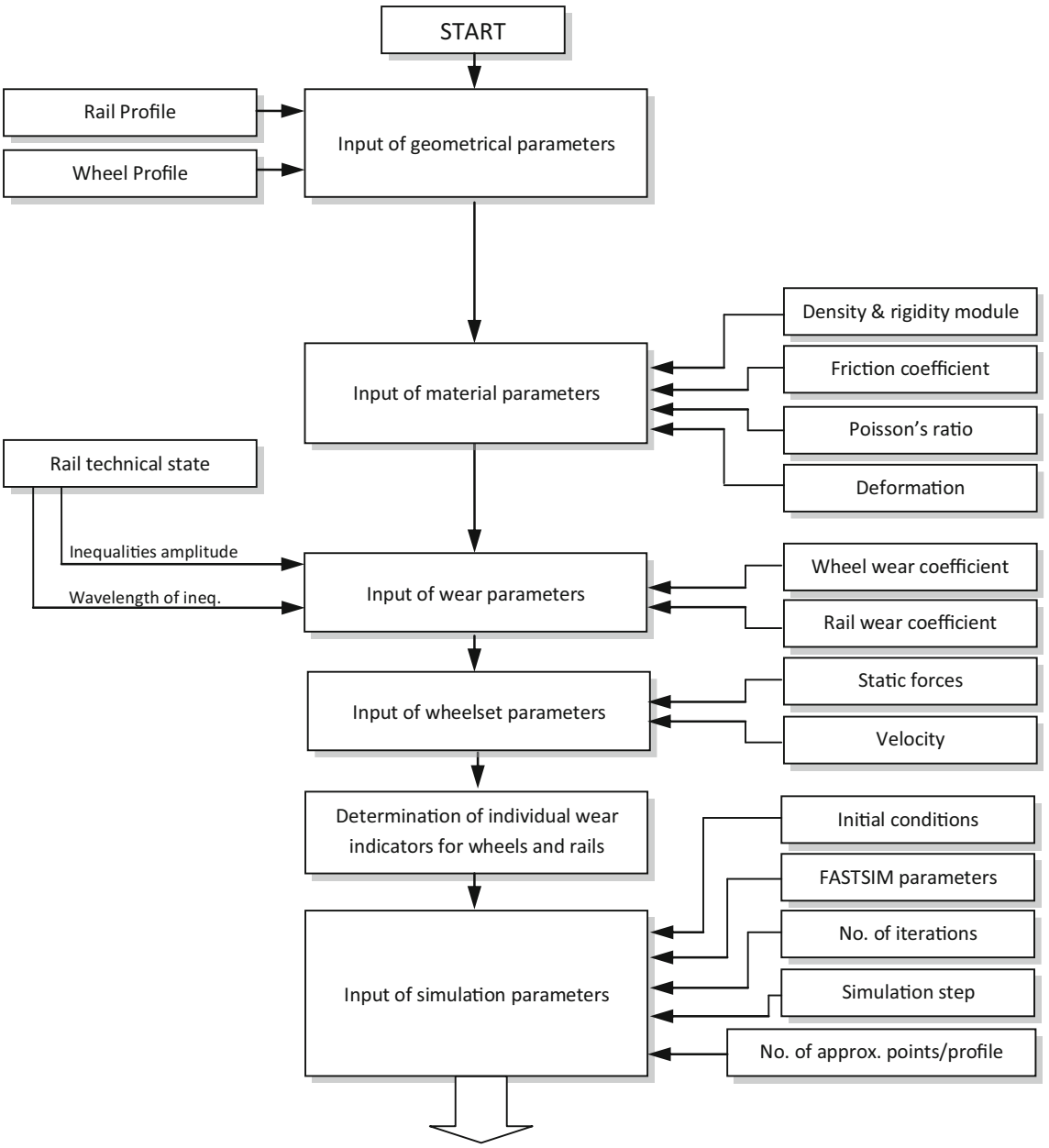

Fig. 10 Simulation model of the wear process—the data preparation module's structure [1]

– Wear characteristics in relation to the distance travelled by the wheel, which is dependent on the rail's condition,
– Generalized wear parameters attributed to the assumed route of the vehicle or averaged to the vehicle's usage period based on the know usage indicator during that period.

In order to evaluate the wear of the studied wheel–rail pair, kinematics and contact geometry were concentrated on according to the following workflow:

– Calculation of the contact surface area for the left and right sides of the track,
– Indication of the coordinates of the contact points of each wheel–rail pair,
– Calculation of the contact forces in each of the contact zones of the wheels and rails in contact, in accordance with generalized Hertzian theory,
– Calculation of the micro-slips occurring during rolling motion,
– Calculation of the usage wear of the wheel and rail.

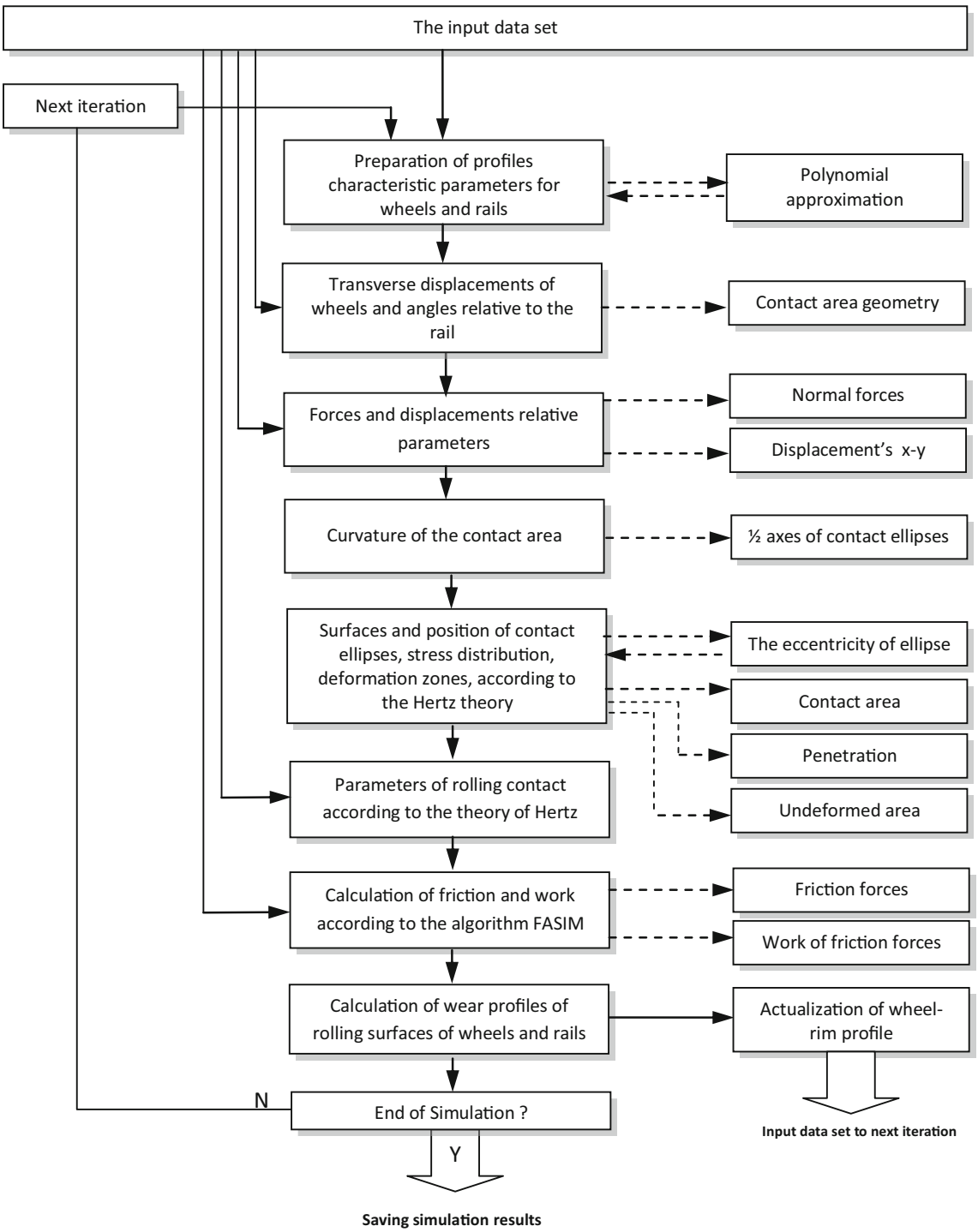

Fig. 11 Simulation model of the wear process—the simulation calculation module's structure [1]

The iterative calculations conducted during the computer simulation allow for the calculation of the location of contact points for the following moments, as well as new and dynamically updating parameters for the contact surfaces of the wheel–rail kinetic pair. The end solution consists of receiving the global wear values for the route travelled by each of the independently spinning wheels.

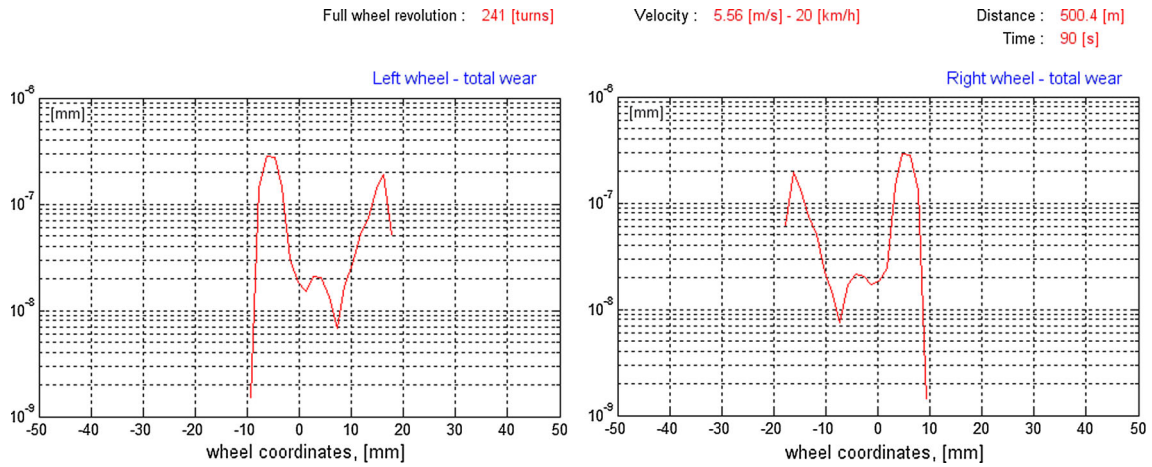

Fig. 12 Wear of wheel rolling surface, segment A, velocity 20 km/h; empty tram, very good condition of track

3.2 The simulation's scenarios

During the studies, a various traveling speed and an empty and loaded state were taken into account. Simulation studies were conducted according to the following scenario:

1. Vehicle speed:	20, 40, 60, 80 km/h
2. Vehicle Load:	no passengers—empty state, all seats and 50% standing spots occupied—regular usage state (loaded)
3. Track condition:	very good, adequate (sufficient)
4. Rail profile:	S49
5. Studied segment length:	500 m

The subjected vehicle moved across a straight track with inequalities, which represented a very good and sufficient state of track, which they differed amplitude and wavelength of inequality, according to the specifics real experimental studies. The results of the simulation were presented in pairs in a linear and logarithmic scale, in order to smooth out, and better observation the resulting changes.

4 Sample results

Figures 12 and 13 illustrate a selected results received from the wear simulation of the wheel rolling surfaces of the wheelset of the tram wagon in section A. The studies took into account the 20 km/h speed and the empty or loaded state of the tram. Two track conditions were assumed: very good and adequate; the results of the simulation were presented in pairs in a linear and logarithmic scale, in order to smooth out the resulting changes.

For the presented above scenario, an absence of wear occurring on the wheel rims was found for the track in very good condition, regardless of the state of usage load. Two wear zones occur on the wheel rolling surfaces (the coordinate of the left wheel's rolling surface being within -8 to -5 mm and within 15–20 mm, symmetrically for the right wheel), and the amount of wear in these points does not exceed 3×10^{-7}mm.

The wear of the rolling surface is around twice as great in the case of an sufficient track condition, and the profile wear surface then distinctly widens. The wear of the rim always occurs on adequate condition track and shapes itself around the value of 3×10^{-6}mm, regardless of load.

Figures 14, 15, and 16 present a summary of the study results for motion over a straight track, in accordance with the study scenarios presented before. The distinguishes:

$L_{\max}$, $R_{\max}$	Maximal wear of the left and right wheel profile,
$\mathrm{LPT}_{\max}$, $\mathrm{RPT}_{\max}$	Maximal wear of the rolling surface of the left and right wheel.

Figures 14 and 15 present a listing of the results received from the wear simulation of the wheel rolling surfaces of the wheelset of the tram wagon in sections A, C, E. The studies took into account the 20 km/h speed and the empty and loaded state of the tram. Only sufficient track conditions were assumed.

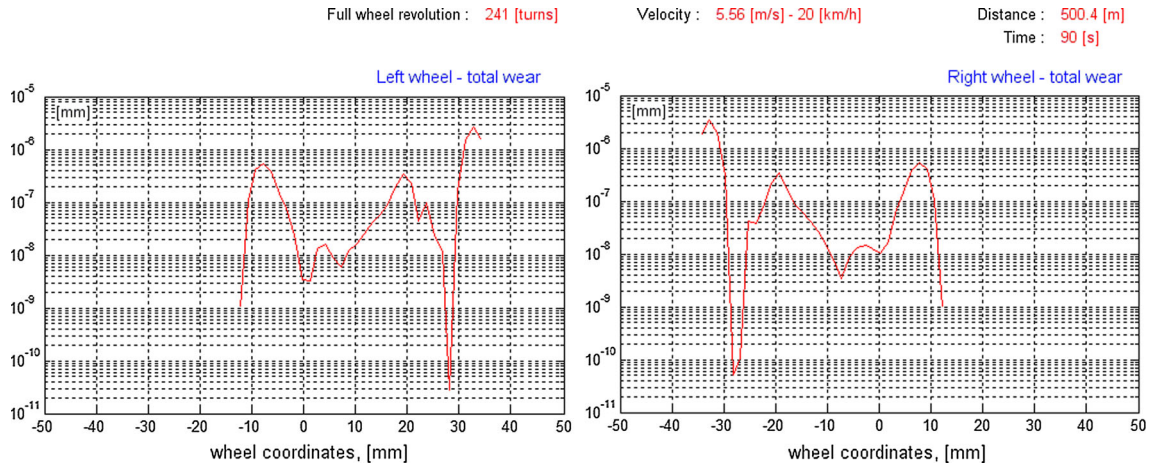

Fig. 13 Wear of wheel rolling surface, segment A, velocity 20 km/h; loaded tram, sufficient condition of track

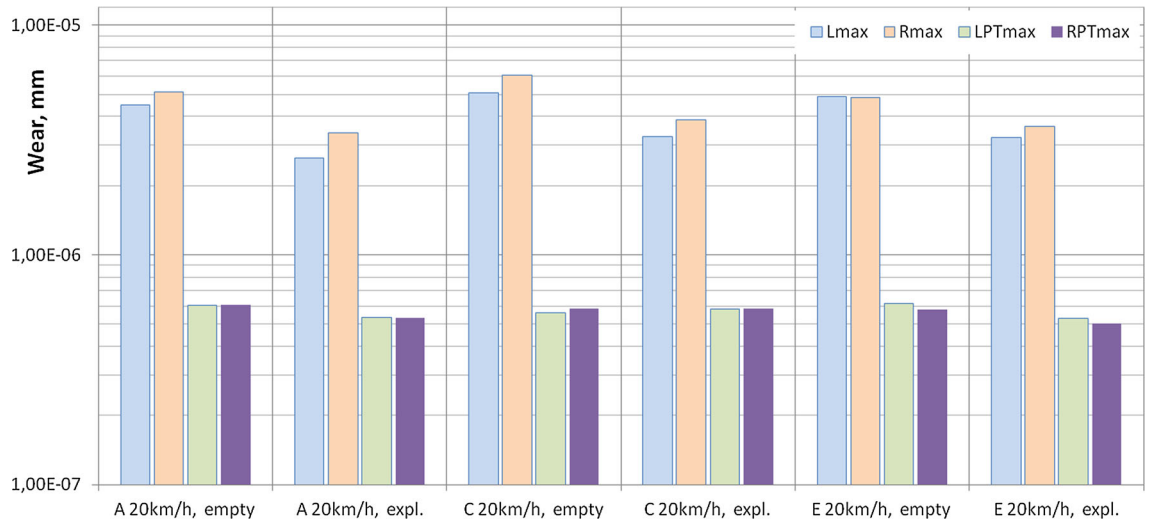

Fig. 14 Wear of wheel rolling surfaces, segments A, C, E, velocity 20 km/h; loaded and empty tram, sufficient state of rail

The wear of the rim of the wheel is around eightfold greater as in the case the rolling surface, regardless of the position of the wheelset, during testing at a sufficient maintenance condition of the track. This can have a connection with behavior of IRW wheelsets. IRW has tend to make an oscillatory motion, which is probably not an effect of the phenomenon described by Klingel. Inequalities of the track have a large influence on the trajectory.

As shown in Fig. 15, the phenomenon of increased disproportion, the wear increases with the speed of the tram. The wear of the rim of the wheel is around tenfold greater as in the case the rolling surface, regardless of the position of the wheelset, during testing at a sufficient maintenance condition of the track, by the speed 80 km/h. Figure 16 presents a listing of the results received from the wear simulation of the wheel rolling surfaces of the wheelset of the tram wagon in section A, for four typical speeds (described in scenario section), and for the empty and loaded state of the tram, for sufficient track conditions.

For the scenarios presented above, wear occurred on the wheel rims for any track condition with an empty load during the simulation studies. Two greater wear zones occur on the wheel rolling surfaces regardless of load. The wear of the rim always occurs on sufficient condition of track and shapes itself between the value of 4×10^{-6} mm and 8×10^{-6} mm with no load, and between 2×10^{-6} mm and 5×10^{-6} mm with exploitation load.

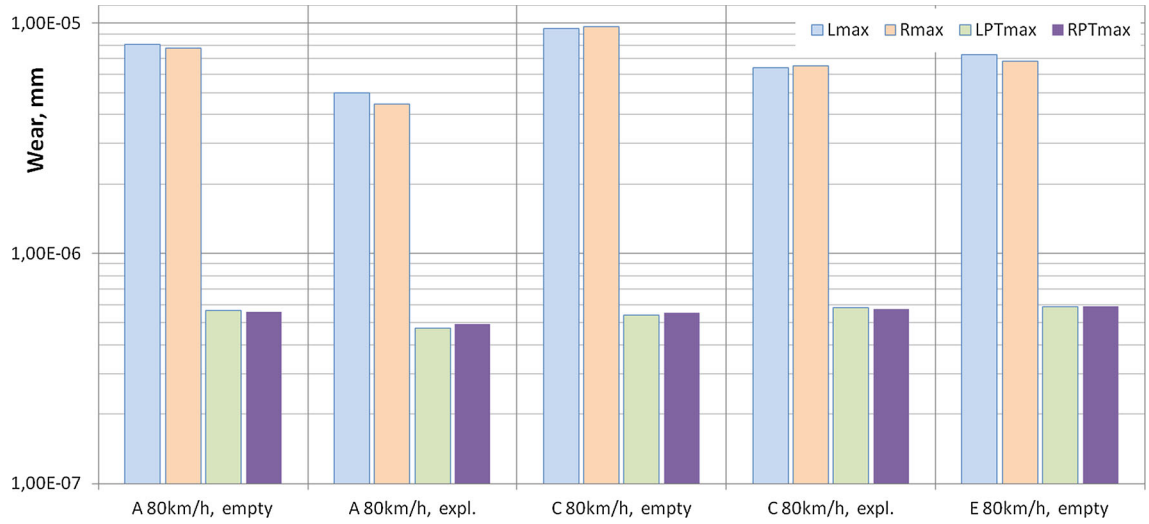

Fig. 15 Wear of wheel rolling surfaces, segments A, C, E, velocity 80 km/h; loaded and empty tram, sufficient state of rail

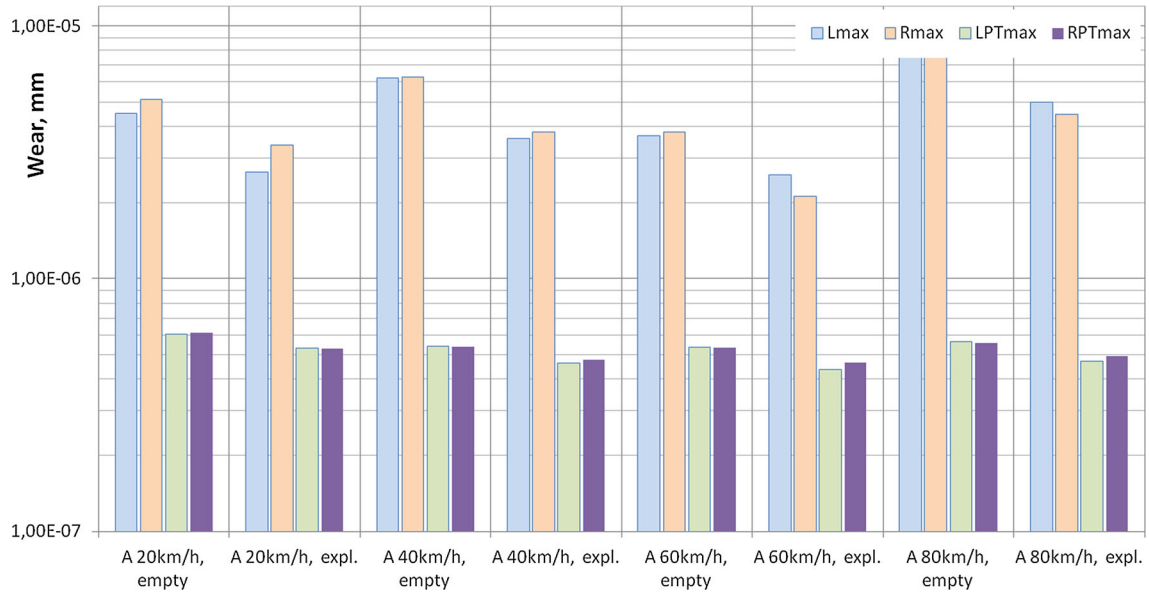

Fig. 16 Wear of wheel rolling surface, segment A, velocities 20–80 km/h; loaded and empty tram, sufficient state of track

5 Concluding remarks

Simulation studies were designed to evaluate the dynamics of the vehicle under various operating conditions, depending on: state of the track, its configuration and speed of the vehicle. Multi-variant calculations, that incorporate different operating scenarios, allowed to evaluate the wear of wheel rolling surface, preceding the introduction to exploitation of the new model of tram bogie, equipped with independently rotating wheels.

In the simulation studies, no wheel rolling plane wear greater than 6e−7 mm was observed, which is in accordance with the data found in the subject literature. This wear was recorded for a minimum speed of 20 km/h, in a state of loaded with passengers and with an sufficient track condition.

The wear of the wheel rims in the case of sufficient track maintenance state with a regular passenger load, at a speed of 80 km/h was at its greatest, and amounted to 9.63e−6 mm, and is around tenfold greater as in the case the rolling surface, regardless of the position of the wheelset (A, C, E).

Acknowledgements This work was supported in part by the Research Funds Demonstrator + (NCBiR) and was registered as research Project under the Grant No. WND-DEM-1-493/00.

References

1. Chudzikiewicz, A., et al.: The structural design of a modern, completely low-floor tram with independently rotating wheels (Report in Polish) NCBiR—DEMONSTRATOR+, Warsaw University of Technology Faculty of Transport—PESA Bydgoszcz (2014)
2. Korzeb, J.: (2013) Prediction of selected dynamic impacts in the transport infrastructure impact zone, monograph in Polish (Predykcja wybranych oddziaływań dynamicznych w strefie wpływu infrastruktury transportowej). In: Scientific Papers of Warsaw University of Technology, Transport Series, No. 90, ISSN 1230-9265, ISBN 978-83-7814-111-2, WUoTPH, Warsaw
3. Korzeb, J., Chudzikiewicz, A.: Evaluation of the vibration impacts in the transport infrastructure environment. Arch. Appl. Mech. **85**(9), 1331–1342 (2015). https://doi.org/10.1007/s00419-015-1029-0
4. Chudzikiewicz A. et al.: (2012) Monitoring of railway vehicle-track system dynamic, monograph in Polish (Monitorowanie stanu ukladu dynamicznego pojazd szynowy-tor). ISBN 978-83-7814-050-4, WUoTPH, Warsaw
5. Chudzikiewicz, A.: Modelling of wheel and rail wear. Arch. Trans. **13**(2), 5–24 (2001)
6. Kalker, J.J., Chudzikiewicz, A.: Calculation of the evolution of the form of a railway wheel profile through wear. Int. Ser. Numer. Math. **101**, 71–84 (1991)
7. Hebda M., Wachal A.: Tribology (in Polish Trybologia), WNT, Warszawa (1980)
8. Lewis, R., Cavalletti, M., Dwyer-Joyce, R.S., Ward, A., Bruni, S., Knani, K. Bel, Bologna P.: Railway wheel wear predictions with adams/rail. In: Report of European Community funded project HIPERWheel (contract number: G3RD-CT2000-00244)
9. Magel, E.: Rolling Contact Fatigue: A Comprehensive Review. U.S. Department of Transportation, FRA (2011)
10. Opala, M.: The method of analysis of active safety rail vehicles (in Polish Metoda analizy bezpieczeństwa czynnego pojazdów kolejowych) (2015), OWPW. ISBN 978-83-7814-358-1, 134 s
11. Piotrowski, J., Kik, W.: Simplified model of wheel/rail contact mechanics for non-Hertzian problems and its application in rail vehicle dynamic simulations. Veh. Syst. Dyn. **46**(102), 27–48 (2008)
12. Sokolski, P., Ziemba, S.: Wear caused by friction machine parts (in Polish Zużycie elementów maszyn spowodowane tarciem), Warszawa PWN (1969)
13. Chudzikiewicz, A., Droździel, J., Sowiński, B.: Mathematical Model of Track Settlement Caused by Dry Friction, Archives of Transport, 3–4 (2009)
14. Johnson, K.L.: Contact Mechanics, Cambridge University Press, 9th printing (2003)
15. Olofsson, U., Zhu, Y., Abbasi, S., Lewis, R., Lewis, S.: Tribology of the wheel–rail contact—aspects of wear, particle emission and adhesion. Veh. Syst. Dyn. Int. J. Veh. Mech. Mob. **51**(7), 1091–1120 (2013). https://doi.org/10.1080/00423114.2013.800215
16. Adamiec, P., Witaszek, M., Witaszek, K.: The intensity of steel wear of railway the wheel rims (in Polish Intensywność zużycia stali na obręcze kółkolejowych). Zeszyty Naukowe. Transport z. 30/ Politechnika Śląska, ISSN 0209-3324. 1998, str. 71–78
17. Aniołek, K., Herian, J.: Load and wear railway turnouts in operating conditions and materials used in their construction (in Polish Obciążenie i zużycie rozjazdów kolejowych w warunkach eksploatacyjnych oraz materiały stosowane do ich budowy). TTS 2-3/2013 2-3/2013, str. 85–96
18. Archard, J.F.: Contact and rubbing of flat surfaces. J. Appl. Phys. **24**, 981–988 (1953)
19. Chudzikiewicz, A.: Symbolic modeling in simulation research of rail vehicle. Arch. Trans. **9**(3–4), 15–25 (1998)
20. Brodny J.: Friction modeling in mechanical systems (in Polish Modelowanie Tarcia W Układach Mechanicznych), Górnictwo I Geologia, : Tom 5 Zeszyt 2. Politechnika Śląska, Gliwice (2010)
21. Duda, S.: Modelowanie i symulacja oddziaływań dynamicznych koło—szyna w ruchu pojazdu w rozjeździe kolejowym. Modelowanie Inżynierskie nr 45, t. 14, rok 2012. ISSN 1896-771X, str. 32–38
22. Kusiak, C.: Adhesion of metals and relaxation friction. Tribology: friction, wear, lubrication (in Polish Adhezja metali i relaksacja siły tarcia. Tribologia : tarcie, zużycie, smarowanie), ISSN 0208-7774, Nr 3, 2008, Wyd. SITMP, pp. 333–338
23. Zając, G., Jurga, S.: Durability testing the wheel rims tram operated in MPK SA in Cracow (in Polish Badania trwałości obręczy kółtramwajowych eksploatowanych w MPK S.A. w Krakowie). Problemy Eksploatacji Nr 2-2009, pp. 139–148
24. Bowden, F.P., Tabor, D.: Mechanism of metallic friction. Nat. **150**, 197–199 (1942). https://doi.org/10.1038/150197a0
25. Tomlinson, G.A.: Molecular theory of friction. Lond. Edinb. Dublin Philos. Mag. J. Sci. **7**(46), 905–939 (1929). https://doi.org/10.1080/14786440608564819
26. Dieriagin, B.W.: What is the friction (in polish: Co to jest tarcie). PWN, Warsaw, Poland (1956)
27. Kragelski, I.: Some concepts and definitions which apply to friction and wear. Acad. Sci. USSR, Moscow (1957)
28. Kostetski, B.I.: Essence of the phenomena of friction and wear in machine components. In: Proceedings of Second Conference on Friction and Wear, vol. 4, pp. 201–208. Acad. Sci. USSR, Moscow (1951)
29. Chudzikiewicz, A., Kalker, J.J.: Wheel–rail wear calculations with the FASTSIM routine. Arch. Trans. **1**(1–2) (1989)
30. Sun, Y.-H., Chen, T., Wu, C.Q., Shafai, C.: Comparison of four friction models: feature prediction. J. Comput. Nonlinear Dyn. ASME Digital Collection, vol. 11 (2016) https://doi.org/10.1115/1.4031768
31. Enblom, R.: Deterioration mechanisms in the wheel–rail interface with focus on wear prediction: a literature review. Veh. Syst. Dyn. Int. J. Veh. Mech. Mob. **47**(6), 661–700 (2009). https://doi.org/10.1080/00423110802331559
32. Kalker, J.J.: Fast algorithm for the simplified theory of rolling contact. (FASTSIM program). In: Vehicle System Dynamics, vol. 11, pp. 1–13. Swets & Zeitlinger B.V. Lisse (1982)